PAPER • **OPEN ACCESS**

What governs the atomic structure of the interface between 2D transition metal dichalcogenides in lateral heterostructures?

To cite this article: Francis H Davies *et al* 2024 *2D Mater.* **11** 015003

2D Materials

OPEN ACCESS

RECEIVED
23 May 2023

REVISED
22 September 2023

ACCEPTED FOR PUBLICATION
6 October 2023

PUBLISHED
19 October 2023

PAPER

What governs the atomic structure of the interface between 2D transition metal dichalcogenides in lateral heterostructures?

Francis H Davies[1,*], **Kai Mehlich**[2], **Carsten Busse**[2] and **Arkady V Krasheninnikov**[1,3,*]

[1] Institute of Ion Beam Physics and Materials Research Helmholtz-Zentrum Dresden-Rossendorf, 01328 Dresden, Germany
[2] Department of Physics, Universität Siegen, 57068 Siegen, Germnay
[3] Department of Applied Physics, Aalto University, PO Box 11100, FI-00076 Aalto, Finland
[*] Authors to whom any correspondence should be addressed.

E-mail: f.davies@hzdr.de and a.krasheninnikov@hzdr.de

Keywords: transition metal dichalcogenides, *ab initio* calculations, lateral heterostructures

Supplementary material for this article is available online

Abstract

The development of lateral heterostructures (LHs) based on two-dimensional (2D) materials with similar atomic structure but distinct electronic properties, such as transition metal dichalcogenides (TMDCs), opened a new route towards realisation of optoelectronic devices with unique characteristics. In contrast to van der Waals vertical heterostructures, the covalent bonding at the interface between subsystems in LHs is strong, such that the morphology of the interface, which can be coherent or contain dislocations, strongly affects the properties of the LH. We predict the atomic structure of the interface with account for the mismatch between the primitive cell sizes of the components, and more important, the widths of the joined materials using parameters derived from first-principles calculations. We apply this approach to a variety of TMDCs and set a theoretical limit on when the transition of the interface from coherent to dislocation-type should occur. We validate our theoretical results by comparison with the initial stage of two-dimensional heteropitaxial growth of junctions between MoS_2 and TaS_2 on Au(111).

1. Introduction

The ability to combine two-dimensional (2D) materials with diverse properties and to develop both vertical [1–5] (VHs) and lateral [6–9] heterostructures (LHs) makes these systems particularly interesting, especially in the context of their applications in optoelectronics [7, 10–17], flexible electronics [18], spintronics [19], piezoelectric devices [20], as well as energy conversion [21] and storage [22]. In VHs, where the materials are placed on top of each other, their characteristics are defined by the relative orientation and stacking order of the 2D sheets, which are held together by weak van der Waals forces. In LH systems, properties are governed by the relative arrangements of the materials within the same plane, and the comparative strength of the interaction between subsystems at the interface. The atomic structure of the interface is also of high importance, especially for the most interesting (in the context of size-quantization effects) case of 'narrow' nanostructures just a few nm wide.

As for the development of LHs, transition metal dichalcogenides (TMDCs) [23] are a highly promising group of 2D materials, as they have similar atomic structure but different chemical composition, which gives rise to their distinct properties. Moreover, they can be synthesised using one-pot molecular beam epitaxy [6, 24] and vapour–solid [7] methods. LHs based on various TMDCs have been successfully prepared [11–13, 25]. Earlier studies predominately showed rough and disordered interfaces [6, 7], with most of them being oriented along the zigzag direction. Continued research effort has improved the growth techniques, and the ability to fabricate sharp interfaces has recently been demonstrated [13, 25, 26].

However, even for sharp interfaces, there remains the problem of lattice mismatch: in general, the equilibrium lattice constants of the individual 2D materials will be different. For pairs with a small lattice mismatch, the junction can be coherent. A large mismatch typically leads to the introduction of dislocations. Indeed, it has been observed that TMDC-based

heterostructures with constituent materials such as MoS_2 and WSe_2 can be created with a coherent or dislocation-type interface depending on the growth conditions [27–29]. Such structures may induce the formation of ripples, although on a larger scale than the interface itself [30] and thus may be neglected. Despite these observations, it is not fully understood what defines the morphology of the interface. In addition to the mismatch in the unit cell sizes of the joined materials and chemical bonding at the interface, the lateral dimensions of the subsystems as well as their overall shape should affect the interface type. For epitaxially grown LHs, also the interaction with the substrate is important.

Here, we focus on the basic physics of the key characteristics, which is the lattice mismatch and how it can be compensated in a coherent or a defective interface. We employ first-principles calculations combined with simple analytical derivations to evaluate the dependency of the interface morphology on mesoscopic structural characteristics of the system. We demonstrate that isomorphic materials have a tendency to form coherent interfaces. We further show that the width of the materials W in the LH is a necessary component for determining whether the interface will form with dislocations or not. We apply this approach to a set of TMDCs and predict when the transition of the interface from coherent to dislocation-type upon increasing W should occur. Finally, we verify our theoretical results by comparison to epitaxially grown LHs of MoS_2 and TaS_2.

2. Methods

In order to investigate the role of strain in lateral interface formation we use first-principles calculations. We apply density-functional theory (DFT) using a plane-wave basis set and the PBE GGA functional [31] along with PAW pseudopotentials [32] as implemented in VASP [33] package. Our calculations use a plane-wave cutoff of 400 eV. For our Monkhorst-Pack grid [34] used in structure relaxations, we applied a minimum of $12 \times 12 \times 1$ points for monolayer TMDCs which are non-periodic in the z-axis. For heterostructures with coherent interfaces the same number of k-points was used in the interface direction. Calculations for large heterostructures with dislocation-type interfaces were performed using the gamma point only.

The dislocation-type LHs were constructed such that each lattice matching (n/m constrained to integers) occurs at a local minimum in strain with increasing length of the period of the interface (see supplementary material for details). This results in less than 0.2% mismatch in all but one case. Although our approach can be applied to any interface type, we concentrate on the zigzag interfaces, as they are energetically more favourable [35, 36] and our experiments also indicate that the interface is of this type.

Sample preparation and analysis was carried out in a home-built ultra high vacuum system equipped with a variable temperature scanning tunnelling microscope (STM). A clean Au(111) substrate was prepared by ion bombardment with Ar^+ at 1.5 keV, first at room temperature for $t = 30$ min, then at $T = 900$ K for $t = 30$ min, followed by an annealing step at $T = 900$ K for $t = 10$ min. This resulted in a clean and well-ordered surface verified using low-energy electron diffraction and STM.

Preparation of the LHs on Au(111) follows a well-established process that was first applied for MoS_2 [37], refined [38], and adjusted for TaS_2 [39]: transition metals were evaporated in an atmosphere of H_2S as the sulphur source. MoS_2 was prepared by first evaporating Mo from an e-beam evaporator (EGCO4 by OAR) with a rate of $R_{Mo} = 0.01\,\mathrm{ML\,min^{-1}}$ for $t_{Mo} = 30$ min onto the substrate held at room temperature (R is determined from the MoS_2 coverage observed in STM and given with respect to a pseudomorphic monolayer (ML) of Mo on Au(111)). Second, H_2S was introduced via a stainless steel tube with a diameter of ≈ 1 cm ending ≈ 3 cm away from the sample. The rate of H_2S was monitored using the chamber pressure measured away from the tube, in this case $P_{H_2S} = 10^{-5}$ mbar. The sample is heated in this atmosphere to $T_{H_2S} = 900$ K for $t_{H_2S} = 20$ min. The gas dosing was continued during natural cool-down and stopped at $T = 450$ K. This leads to extended and defect-free islands of MoS_2 as described previously [40]. We denote the coverage of the TMDC in ML where 1 ML is defined as a substrate fully covered with a single layer. The growth process is repeated for TaS_2 (see also references [41, 42]). We used the same parameters except $R_{Ta} = 0.12\,\mathrm{ML\,min^{-1}}$, $t_{Ta} = 1.5$ min, and $P_{H_2S} = 10^{-6}$ mbar. TaS_2 then forms a rim around the pre-existing MoS_2-islands.

The resulting structures were imaged using STM at room temperature. A bias voltage of -0.5 V was applied to the sample, the setpoint for the tunnelling current was 6 nA. The images were processed using WSxM [43] and Gwyddion [44]. Distortions were corrected using atomically resolved images of the substrate.

3. Results and discussion

Prior to proceeding to the results of the calculations and their comparison to our experiments, we would first like to discuss the qualitative picture. When forming an atomically sharp interface between two narrow strips of isomorphic materials, and especially when the mismatch between primitive cell sizes of the materials is large, a dislocation-type interface can form, as schematically illustrated

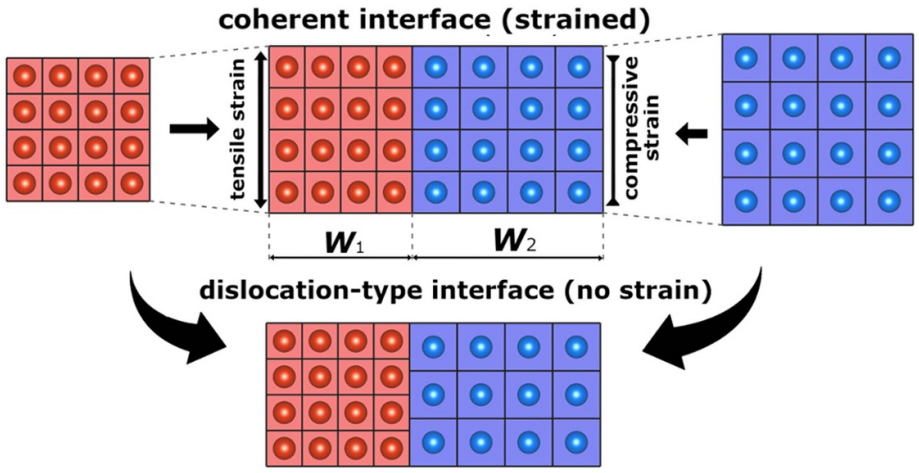

Figure 1. Schematic illustration of possible interfaces which can be formed between two isomorphic 2D materials with different primitive cell sizes. The top interface is coherent with both constituents being strained. The bottom shows a dislocation-type interface, with little or no strain in the constituents. Note that strain energy depends on the width W of the heterostructures.

in figure 1. When the mismatch is small, a coherent interface will be energetically favourable, which seamlessly connects the atomic structures. We stress that the coherent interface has lower interface energy E_{int} (the energy released when two materials are joined together, $E_{\text{int}} < 0$) than the dislocation interface, as the former does not have dangling bonds or under/over-coordinated atoms. As for the latter, the dislocation point is a periodic feature that occurs along the interface dividing regions of local coherence. This is strongly supported by studies demonstrating the growth of channels of MoS_2 into WSe_2 at the low stability dislocation points [27] and this has also been shown for WS_2 channels growing into WSe_2 [45].

The total energy of a LH can be defined as a sum of E_{int} (for the coherent or dislocation-type interface) and elastic strain energy U,

$$E_{\text{tot}} = E_{\text{int}} + U(\mathcal{E}, W)\,. \tag{1}$$

Strain energy in a 2D material is

$$U(\mathcal{E}, W) = \frac{1}{2}\lambda_{\text{t}} W L_0 \mathcal{E}^2, \tag{2}$$

where $\mathcal{E} = \Delta L/L$ is the strain, W and L_0 are the width and initial interface length, respectively. The value of λ_{t} is the thickness-coupled Young's modulus. There is some ambiguity in defining the thickness of a 2D material, we therefore avoided this by considering the Young's modulus and the thickness of the system as a single coupled constant which can be found by DFT calculations. Although the binding energy of the coherent interface is lower than the dislocation-type interface, $E_{\text{int}}^{\text{coh}} < E_{\text{int}}^{\text{dis}}$, strain in the direction parallel to the interface is much larger, $\mathcal{E}^{\text{coh}} \gg \mathcal{E}^{\text{dis}}$. The key point is that the strain energy scales linearly with material width W, while the interface binding energy is independent of W.

Many materials are just moderately incommensurate, therefore, it is reasonable to expect that they can form either a dislocation or coherent interface, and its morphology will be defined by material width. For 'narrow' strips of material, the coherent interface can be energetically favourable, but at some critical width W_{c} the influence of strain energy U becomes larger than the energy gain from forming a coherent interface E_{int}. For the condition that $W > W_{\text{c}}$,

$$E_{\text{int}}^{\text{coh}} + U\left(\mathcal{E}^{\text{coh}}, W\right) > E_{\text{int}}^{\text{dis}} + U\left(\mathcal{E}^{\text{dis}}, W\right) \tag{3}$$

because $\mathcal{E}^{\text{coh}} \gg \mathcal{E}^{\text{dis}}$ and hence $U(\mathcal{E}^{\text{coh}}, W) \gg U(\mathcal{E}^{\text{dis}}, W)$ making the dislocation-type interface energetically preferable.

The discussion above develops out of the established description of 3D-heterostructures. In this context there was a strong focus on thin epitaxial overlayers on suitable substrates. Due to the higher dimensionality here the decisive parameter is the critical layer thickness. As above, for low mismatch a coherent interface is possible (pseudomorphic growth). There are widely used models to predict the critical thickness, notable examples were derived by Matthews and Blakeslee [46], Matthews [47], and van der Merwe [48]. These models rely on assumptions regarding Burgers vectors and glide planes of the dislocations, the cutoff radius for the determination of the dislocation line energy, and approximations of the elastic behaviour. Furthermore, they require input parameters as Young's modulus and Poisson ratio which are often not readily available for 2D materials and have to be extrapolated from the 3D parent compounds (when available) or derived by *ab initio* calculations. Often, the parameters entering the final expressions for the critical thickness in these models

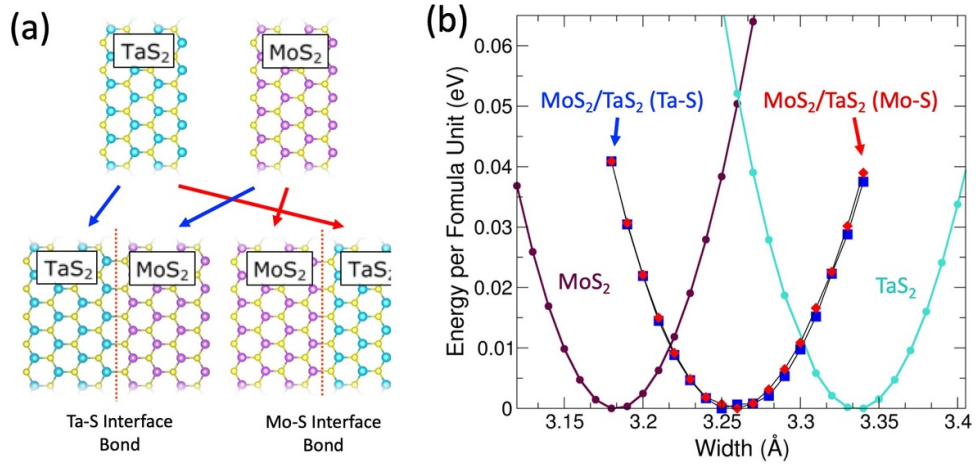

Figure 2. (a) Schematic diagram illustrating how two TMDC nanoribbons can be combined to form two different interfaces. (b) Energy vs strain curves for the two constituents and for the two interfaces. Points represent calculated values and the lines are fitted quadratic curves. The strain is applied along the interface direction.

are obtained by fitting to experimental results. Still, the development of equivalent models for heteroepitaxy of 2D materials is highly desirable as they could allow fast screening of suitable material combinations and geometrical parameters with reduced computational effort. Our calculations based on DFT detailed in the following can serve as a benchmark for future models of this kind.

In order to get microscopic insight into the atomic structure of the interface between different TMDCs, we carried out first-principles calculations as described in the 'Methods' section. We considered a set of five TMDCs and eight heterostructure pairs. All the materials are stable in the 2H phase [49] and cover a range of disparate lattice constants. The investigation for each material and LH proceeds in the same manner, and therefore we will focus on the MoS_2/TaS_2 system as a case study that we can also compare to our experimental results (see below). First we discuss the coherent interface and the intrinsic strain that occurs due to the difference in the lattice constants. However, it is important to recognise that there is more than one form of interface between materials. The different edge structures give rise to different interfaces and (along the zigzag direction) there are two possible terminations, sulphur terminated or transition metal terminated, as seen in figure 2(a). We neglect the energetically less favorable metal-metal and sulphur-sulphur interfaces leaving only the two metal-sulphur interfaces. We choose to limit our search to the zigzag direction because this direction is far more common for TMDC interfaces [25].

A clearly identifiable feature of the interface are the bonds that are formed between the constituents. As shown in figure 2 an interface between TaS_2 and MoS_2 can form either Ta–S or Mo–S interfacial bonds. However, one interface will have a lower formation energy and will therefore be more likely to form. The formation energy of any interface (E_{int}) can be assessed using

$$E_{\text{int}} = E(A+B) - E(A) - E(B)\,, \tag{4}$$

where $E(A+B)$, is the total energy of the fully optimised heterostructure as calculated by DFT. The reference energies, $E(A)$ and $E(B)$, are the total energies for constituent A and B respectively, each examined in the exact structure they adopt when the interface is present, including strain and edge deformation. In the case of MoS_2/TaS_2 the formation energy from isolated ribbons is -1.29 eV Å^{-1} for the Mo–S interfacial bond and -1.10 eV Å^{-1} for the Ta–S interfacial bond. The cohesive energy of MoS_2 is -16.8 eV/formula unit while TaS_2 has -17.7 eV/formula unit demonstrating that the Ta-S bond is stronger. The interface sulphur in Mo–S case is bonded to two Ta ions, a stronger bond, and one Mo ion, a weaker bond, giving rise to the preferable interface. We note, however, that the energetics of the interface depends on many other factors, such as charge transfer and stability of the 'naked' edges. Moreover, in the experiment one of the materials already exists when the second material starts growing.

The periodic length unit of the interface emerges from an equilibrium between the compressive and tensile strains of the two materials. The strain energy curves, depicted in figure 2(b), for the heterostructure, are the summation of individual component strain energies. These curves play a crucial role in calculating the coupled Young's modulus by fitting to equation (2). In our method, each LH with a dislocation interface has a lattice matching that occurs at a local minimum in strain (see supplementary materials) and hence at a local minimum in energy, therefore making them ideal candidates for meta-stable

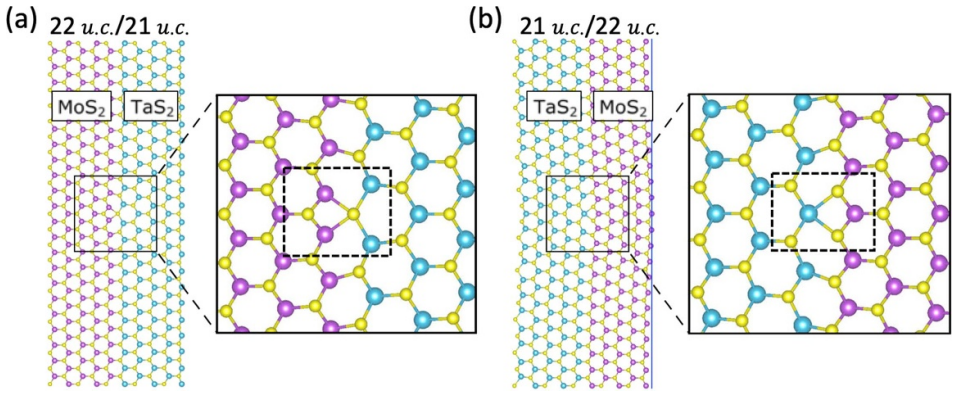

Figure 3. (a) High-constraint dislocation interface and (b) low-constraint dislocation interface. Note the bending of the system after atomic relaxation, as evident from the vertical straight line drawn at the right-hand side. The zoomed images show a closeup of the atomic structure near the dislocation. The corresponding numbers of unit cells (*u.c.*) matched at the interface are shown above the constituents.

configurations. The coherent interface however owes any potential metastability to its lack of dislocations and seeded growth configuration which could lead to further mechanical barriers not evaluated here. To better present the data, we have chosen to assume that the widths of the constituent TMDC ribbons are roughly the same, that is they consist of the same number of unit cells of the corresponding materials. This assumption is made purely for the sake of clarity and simplicity in our presentation and analysis. Leveraging this approach, we can calculate an optimal interface length for any coherent interface as discussed at length in the supplementary material.

The alternative interface can be created using dislocations where effects of strain are negligible. For the dislocation interface calculations we use large supercells of each constituent so that the mismatch between the subsystems can be minimised. Due to computational limitations (the largest systems we considered were composed from ca. 700 atoms) the width of the constituents in our calculations was limited, and the interface was constructed from two finite width nanoribbons. To assess finite-width effects, we used two simulation setups. In the first high-constraint setup the atomic structure at the edges opposite to the interface was forced to remain the same as in the infinite crystal. The other approach was a low-constraint setup which allowed full reconstruction at the edges or even bending of the system. The high-constraint setup will obviously underestimate the interface energy, while the low-constraint system will overestimate it, because it allows for excessive reconstruction. By considering both systems we can confidently identify an upper and lower limit on the interface energy. We further assumed that an average of the two values corresponds to the 'true' interface energy.

Examples of the interfaces between TaS_2/MoS_2 TMDCs calculated using the high- and low-constraint setups are shown in figures 3(a) and (b) respectively. Note that the chemical bonding (Mo–S and Ta–S) at the interface in the structures is different. In both cases the dislocation is localised allowing the structure to approach coherent interface away from the dislocation. In both cases the structure deforms around the dislocation. However, only in the low-constraint system do the ribbon edges deform. The energy of the MoS_2/TaS_2 dislocation interface is found to be in the range of from $-1.26\,\mathrm{eV\,Å^{-1}}$ to $-1.05\,\mathrm{eV\,Å^{-1}}$, and higher (less favourable values) were found for the TaS_2/MoS_2 dislocation interface. From now on we concentrate on the energetically most favourable interface only.

Having assessed the energetics of the dislocation-type interfaces, we combined the results with the energy of the coherent interface and calculated the total energy of the system as a function of the width of the constituents, which were assumed to be the same as each other for the sake of simplicity. We note that the generalisation of the approach to arbitrary width of the subsystems is straightforward.

The elastic energy of a 2D material is proportional to the area of the strained material. As the width of a heterostructure increases, the strain energy grows in accordance with equation (1). However, it grows at different rates for the dislocation-type (which is essentially independent of strain) and coherent interfaces.

In figure 4(a), the energies for the MoS_2/TaS_2 high-constraint and low-constraint dislocation interfaces are plotted against width of the constituent strips. The interface energy is independent of width, therefore those structures with more preferable interfaces are separated by the difference in their interface energy. This places the low-constraint dislocation interface below the high-constraint one and it puts the coherent interface below both. It can be seen that MoS_2/TaS_2 cross over between 8 Å and 56 Å, with the average value being about 30 Å.

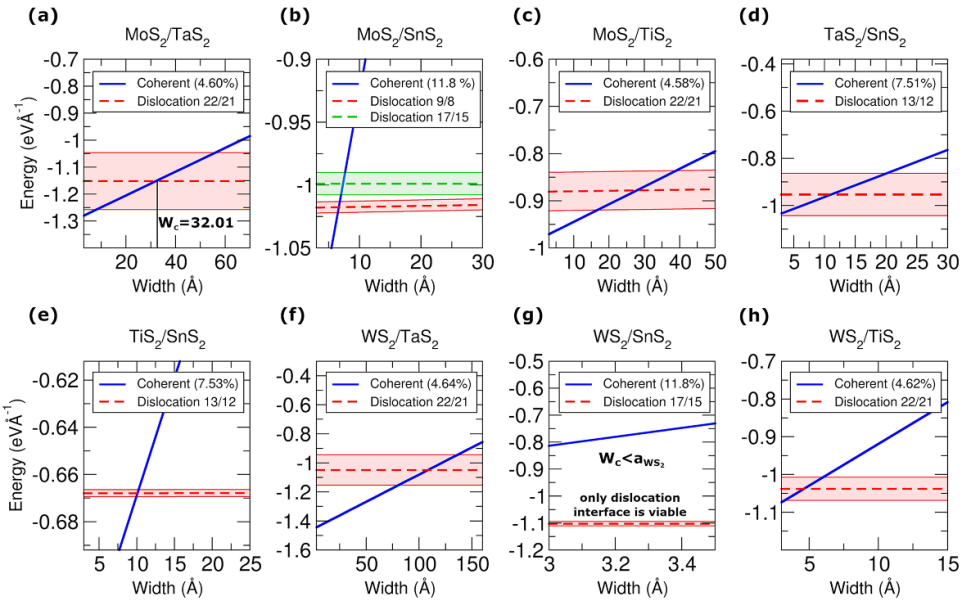

Figure 4. Interface transition graphs with the coherent interface shown as a solid blue line with lattice mismatch indicated in the legend. A dashed-line in red (or green) shows the average dislocation interfaces energies defined by the solid line enclosing the shaded region of corresponding colour. The solid red (green) lines represent the high and low constraint dislocation interfaces. The line with the lowest energy is the energetically favourable structure at that width. The mismatch between the materials primitive cell is given in %, and the number of primitive cell required to make a dislocation-type interface with a strain of less than 0.2% is also indicated. (a) MoS_2/TaS_2 with a transition width of 32 Å, (b) MoS_2/SnS_2 with transitions at 7 Å to 9/8 interface and at 173 Å to 17/15 MoS_2/SnS_2 interface, (c) MoS_2/TiS_2 with a width of 28 Å, (d) TaS_2/SnS_2 with a width of 11 Å, (e) TiS_2/SnS_2 with a width of 10 Å, (f) WS_2/TaS_2 with a width of 110 Å, (g) WS_2/SnS_2 with a width of 1.3 Å, (h) WS_2/TiS_2 with a width of 5 Å.

In figures 4(b)–(h) we present similar data for other materials (see supplementary materials for the corresponding parameters). The transition point W_c defined by equation (3) is different for different material pairs. In particular, figure 4(b) shows the estimate for two dislocation type interfaces of MoS_2/SnS_2; one at 9 to 8 matching and one at a 17 to 15 matching. For both interfaces, the dislocation-type interface becomes energetically preferable already at a width of about one nm, which corresponds to approximately three unit cells. We note that for that system two dislocation-type interfaces with finite values of strain have close energies: the 9 MoS_2 to 8 SnS_2 interface has a lower energy, but the 17 MoS_2 to 15 SnS_2 interface will become more preferable for the system width of about 173 Å (the crossing point is not shown on the plot). This transition, however, does not account for the diffusion barrier for dislocation core migration, additionally at such scales ripples in the sheets could very well compensate for the strain obviating the need for the 17/15 matching.

The same methodology used for MoS_2/TaS_2 can be applied to other material as shown in figures 4(c)–(f). Each system exhibits the same pattern, with the dislocation interface dominating at large widths and the coherent interface becoming more preferable at lower widths. For some of the heterostructures, such as WS_2/SnS_2, the theoretical transition point is smaller than the lattice constant. This means that the coherent interface is unlikely to exist for this pair of materials.

Although our theory treats freestanding LHs, it is also a good approximation for supported structures when the interaction with the substrate is weak and governed by van der Waals forces [6, 7, 24, 26]). For a full treatment of epitaxially grown LHs, however, the interaction with the substrate should be accounted for. Moreover, the interaction of 2D materials with the substrate depends on the roughness and cleanliness of the substrate [50].

To experimentally validate our first-principles calculations, we have studied the initial phase of 2D heteroepitaxial growth in the model system MoS_2/TaS_2 on Au(111), which is a substrate that only weakly interacts with the supported TMDC monolayers as evidenced by the incommensurability of the superstructures, a rather large vertical separation [40, 41] and the only slightly perturbed electronic structure of the overlayers [39, 51]. To be quantitative, using TaS_2 as an example: The S atoms in the lower layer bind to the Au atoms below with an average bond strength of 0.02 eV/bond [41], whereas the strength of the in-plane bonds in TaS_2 can be estimated from the cohesive energy calculated by us to be 3.9 eV/bond. Therefore we assume that the structural properties are fully governed by the in-plane bonds.

After the first step with the growth protocol detailed in 'Methods', the surface is covered by hexagonal monolayer MoS_2 islands with a coverage of 0.3 ML, a mean distance of 80 Å and an average diameter of 50 Å. The TaS_2 prepared in the second step strongly prefers to attach to the pre-existing

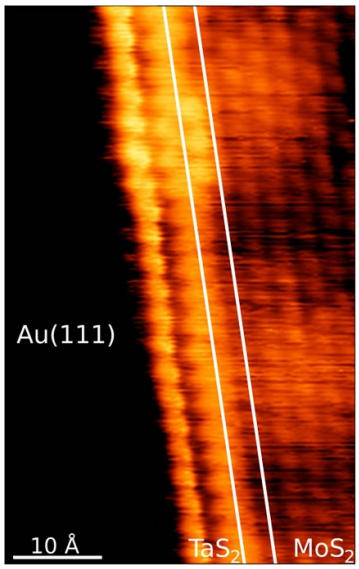

Figure 5. Scanning tunnelling microscopy image of a lateral heterostructure formed by monolayer MoS_2 (right) and TaS_2 (middle) on Au(111) (left).

MoS_2 islands instead of nucleating a separate phase. We observe more triangular heterostructure islands with a mean side length of 130 Å. Figure 5 shows the LH formed at the edge of such an island where the MoS_2 core is encased in a TaS_2 shell. Exploiting the slight asymmetry of hexagonal MoS_2 islands on Au(111) [52], we can infer that the interface is of Mo-S type (see figure 2(a)), which is the energetically preferred interface studied in detail in the theoretical section.

The bright protrusions in figure 5 are individual S atoms from the upper sulphur layer, forming the characteristic hexagonal lattice. MoS_2 appears slightly lower due to the reduced density of states around the Fermi level. While it is obvious that the first two rows are TaS_2, and from row four there is TaS_2 the nature of the third row is ambiguous. Either there is some intermixing or there are special electronic states directly at the junction that alter the appearance in STM. The large-scale modulation in contrast seen on MoS_2 is the moiré superstructure arising from the lattice mismatch between the 2D materials and the substrate [40]. This moiré pattern enables a precise determination of the MoS_2 lattice constant, and we obtain (3.15 ± 0.01) Å, which agrees with the value found for pristine MoS_2/Au(111) [40]. The section of the LH visible in figure 5 has a length of 21 lattice constants. The atomic rows perpendicular to the interface are continuous, there is no dislocation visible. We analysed numerous LHs on the sample and did not find a single dislocation, so the interface between MoS_2 and TaS_2 is coherent. This implies that the TaS_2 (experimental lattice constant (3.30 ± 0.01) Å [41]) fully adjusts to MoS_2 and is thus compressed by $\approx 5\%$.

Our finding of an unaltered lattice constant for MoS_2 is expected for a thin shell of TaS_2 around a much wider MoS_2 core. This experimental situation is closely related to the study of 3D-heteroepitaxial growth, where most often an unstrained substrate is assumed. For comparison with our theoretical treatment, we can consequently take the limit $W_{MoS_2} \to \infty$. This leads to $6\,\text{Å} < W_c < 42\,\text{Å}$, indicating that thermodynamics allows that the first rows of TaS_2 grow coherently on the 2D MoS_2 substrate, in agreement with our experiment.

In preliminary experiments going beyond the initial stage of 2D heteroepitaxy in this system, we still did not observe the introduction of dislocations, indicating a metastable situation where potentially the introduction of defects is kinetically hindered. We find strain patterns that strongly depend on growth conditions and overall morphology of the heterostructure islands such as size, shape, and vicinity to substrate defects like step edges. A detailed experimental study will be presented in a forthcoming paper.

4. Conclusions

In summary, we can predict the interface type upon the formation of a LH based on TMDCs with consideration of the width of the constituent materials. Further, we applied our approach to a set of different material pairs. We have identified that for any system, the coherent interface is initially preferable but will break down into the dislocation interface at greater width of the constituent strips of the materials. In some cases structures can be expected to become stuck in a metastable state, thus maintaining a coherent interface beyond the point that it is structurally favourable. However, when the transition occurs on length scales shorter than the corresponding lattice constant this effectively eliminates the possibility of the coherent interface forming all together. The methodology developed here is applicable to any pair of 2D materials that share the same atomic symmetry. It can also be generalised to account for the actual growth process, such as the situation when at the beginning of the synthesis of the LH the first material is formed, so that at the coherent interface the strain will be predominantly in the second (growing) material, but not equally distributed. Overall, our results set the theoretical limit on the width of the LH with the coherent interface and thus should help avoid the formation of dislocations at the interface and therefore prevent additional electronic scattering at the interface.

Data availability statement

The theoretical results can be reproduced with the code VASP using the information given in the paper. The input files and the coordinates of the optimized structures can also be give on request. The experimental raw/processed data cannot be shared at this

time, as the data also forms a part of an ongoing study, but it will be shared later.

Acknowledgments

We acknowledge funding from the German Research Foundation (DFG), Project KR 4866/9-1and the collaborative research center 'Chemistry of Synthetic 2D Materials' SFB-1415-417590517. The computational support from the Technical University of Dresden computing cluster (TAURUS) and the High Performance Computing Center (HLRS) in Stuttgart, Germany, is gratefully appreciated. We also thank Dr M Ghorbani-Asl for fruitful discussions.

Conflict of interest

The authors declare that they have no known competing financial interests or personal relationships that could have appeared to influence the work reported in this paper.

ORCID iDs

Francis H Davies https://orcid.org/0000-0003-0786-2773
Carsten Busse https://orcid.org/0000-0001-5522-0578
Arkady V Krasheninnikov https://orcid.org/0000-0003-0074-7588

References

[1] Geim A K and Grigorieva I V 2013 *Nature* **499** 419–25
[2] Miao S *et al* 2021 *Nat. Commun.* **12** 3608
[3] Song J C and Gabor N M 2018 *Nat. Nanotechnol.* **13** 986–93
[4] Liu K, Zhang L, Cao T, Jin C, Qiu D, Zhou Q, Zettl A, Yang P, Louie S and Wang F 2014 *Nat. Commun.* **5** 4966
[5] Chakraborty C, Goodfellow K M, Dhara S, Yoshimura A, Meunier V and Vamivakas A N 2017 *Nano Lett.* **17** 2253–8
[6] Sahoo P K, Memaran S, Xin Y, Balicas L and Gutiérrez H R 2018 *Nature* **553** 63–67
[7] Huang C, Wu S, Sanchez A M, Peters J J, Beanland R, Ross J S, Rivera P, Yao W, Cobden D H and Xu X 2014 *Nat. Mater.* **13** 1096–101
[8] Zheng C *et al* 2017 *ACS Nano* **11** 2785–93
[9] Yu H, Kutana A and Yakobson B I 2016 *Nano Lett.* **16** 5032–6
[10] Withers F *et al* 2015 *Nat. Mater.* **14** 301–6
[11] Levendorf M P, Kim C J, Brown L, Huang P Y, Havener R W, Muller D A and Park J 2012 *Nature* **488** 627–32
[12] Ci L *et al* 2010 *Nat. Mater.* **9** 430–5
[13] Wang J, Li Z, Chen H, Deng G and Niu X 2019 *Nano-Micro Lett.* **11** 1–31
[14] Chen T, Sheng Y, Zhou Y, Chang R I, Wang X, Huang H, Zhang Q, Hou L and Warner J H 2019 *ACS Appl. Mater. Interfaces* **11** 6421–30
[15] Deng W, Chen Y, You C, Liu B, Yang Y, Shen G, Li S, Sun L, Zhang Y and Yan H 2018 *Adv. Electron. Mater.* **4** 1800069
[16] Lin Y C *et al* 2015 *Nat. Commun.* **6** 7311
[17] Luo L L, Wang P X, Geng X Y, Liu Y T, Eglitis R I, Xia H Q, Lai X Y and Wang X 2022 *Phys. Chem. Chem. Phys.* **24** 8529–36
[18] Georgiou T *et al* 2013 *Nat. Nanotechnol.* **8** 100–3
[19] Sierra J F, Fabian J, Kawakami R K, Roche S and Valenzuela S O 2021 *Nat. Nanotechnol.* **16** 856–68
[20] Puthirath A B *et al* 2022 *Adv. Mater.* **34** 2206425
[21] Lee C H *et al* 2014 *Nat. Nanotechnol.* **9** 676–81
[22] Li Y, Zhang J, Chen Q, Xia X and Chen M 2021 *Adv. Mater.* **33** 2100855
[23] Kolobov A and Tominaga J 2016 *Two-Dimensional Transition Metal Dichalcogenides* (Springer)
[24] Zhang Y, Yin L, Chu J, Shifa T A, Xia J, Wang F, Wen Y, Zhan X, Wang Z and He J 2018 *Adv. Mater.* **30** 1803665
[25] Ávalos-Ovando O, Mastrogiuseppe D and Ulloa S E 2019 *J. Phys.: Condens. Matter* **31** 213001
[26] Pielić B, Novko D, Šrut Rakić I, Cai J, Petrović M, Ohmann R, Vujičić N, Basletić M, Busse C and Kralj M 2021 *ACS Appl. Mater. Interfaces* **13** 50552–63
[27] Han Y, Li M Y, Jung G S, Marsalis M A, Qin Z, Buehler M J, Li L J and Muller D A 2018 *Nat. Mater.* **17** 129–33
[28] Li M Y *et al* 2015 *Science* **349** 524–8
[29] Lin Y C, Karthikeyan J, Chang Y P, Li S, Kretschmer S, Komsa H P, Chiu P W, Krasheninnikov A V and Suenaga K 2021 *Adv. Mater.* **33** 2007819
[30] Han Y, Nguyen K, Cao M, Cueva P, Xie S, Tate M W, Purohit P, Gruner S M, Park J and Muller D A 2018 *Nano Lett.* **18** 3746–51
[31] Perdew J P, Burke K and Ernzerhof M 1996 *Phys. Rev. Lett.* **77** 3865–8
[32] Kresse G and Joubert D 1999 *Phys. Rev.* B **59** 1758–75
[33] Kresse G and Furthmüller J 1996 *Comput. Mater. Sci.* **6** 15–50
[34] Pack J D and Monkhorst H J 1977 *Phys. Rev.* B **16** 1748–9
[35] Cao D, Shen T, Liang P, Chen X and Shu H 2015 *J. Phys. Chem.* C **119** 4294–301
[36] Schweiger H, Raybaud P, Kresse G and Toulhoat H 2002 *J. Catalysis* **207** 76–87
[37] Helveg S, Lauritsen J V, Lægsgaard E, Stensgaard I, Nørskov J K, Clausen B S, Topsøe H and Besenbacher F 2000 *Phys. Rev. Lett.* **84** 951
[38] Grønborg S S, Ulstrup S, Bianchi M, Dendzik M, Sanders C E, Lauritsen J V, Hofmann P and Miwa J A 2015 *Langmuir* **31** 9700
[39] Sanders C E, Dendzik M, Ngankeu A S, Eich A, Bruix A, Bianchi M, Miwa J A, Hammer B, Khajetoorians A A and Hofmann P 2016 *Phys. Rev.* B **94** 081404
[40] Silva C C *et al* 2022 *2D Mater.* **9** 025003
[41] Silva C C *et al* 2021 *Phys. Rev.* B **104** 205414
[42] Dombrowski D, Samad A, Murray C, Petrović M, Ewen P, Michely T, Kralj M, Schwingenschlögl U and Busse C 2021 *ACS Nano* **15** 13516
[43] Horcas I, Fernández R, Gómez-Rodríguez J M, Colchero J, Gómez-Herrero J and Baro A M 2007 *Rev. Sci. Instrum.* **78** 013705
[44] Nečas D and Klapetek P 2012 *Cent. Eur. J. Phys.* **10** 181–8
[45] Zhou W, Zhang Y Y, Chen J, Li D, Zhou J, Liu Z, Chisholm M F, Pantelides S T and Loh K P 2018 *Sci. Adv.* **4** eaa9096
[46] Matthews J W and Blakeslee A E 1974 *J. Cryst. Growth* **27** 118
[47] Matthews J 1975 *Epitaxial Growth, Part B* (Academic)
[48] van der Merwe J H 1962 *J. Appl. Phys.* **34** 123
[49] Chhowalla M, Shin H S, Eda G, Li L J, Loh K P and Zhang H 2013 *Nat. Chem.* **5** 263
[50] Velicky M *et al* 2020 *J. Phys. Chem. Lett.* **11** 6112–8
[51] Miwa J A, Ulstrup S, Sørensen S G, Dendzik M, Grubišić Čabo A, Bianchi M, Lauritsen J V and Hofmann P 2015 *Phys. Rev. Lett.* **114** 046802
[52] Krane N, Lotze C and Franke K J 2018 *Surf. Sci.* **678** 136–14